J. Bangladesh Acad. Sci. 48(1); 99-109: June 2024 DOI:https://doi.org/10.3329/jbas.v48i1.71278

Journal of Bangladesh Academy of Sciences

Journal homepage: http://www.bas.org.bd/publications/jbas.html

Research Article

Comparison of non-monotonic and monotonic potentials for cross-sections and analyzing powers of ^{6}Li elastic scattering on ^{12}C at 30 MeV

M. Sujan Islam*, M. Rubel Alamin[1], M. A. Sattar, Shefael K Joarder[2], A. S. B. Tariq[2] and A. K. Basak[2]

Department of Physics, Hajee Mohammad Danesh Science and Technology University, Dinajpur, Bangladesh

ARTICLE INFO

Article History

Received: 30 January 2024
Revised: 19 March 2024
Accepted: 28 March 2024

Keywords: Elastic scattering, Optical model, Energy density function, Non-monotonic, Monotonic

ABSTRACT

The experimental angular distributions of differential cross-section (CS), vector analyzing power (iT_{11}) and tensor analyzing powers (T_{20}, T_{21}, and T_{22}) for the ^{12}C(^{6}Li, ^{6}Li)^{12}C elastic scattering at laboratory energy of 30 MeV are simultaneously analyzed in the structure of simple optical model (OM) using shallow Non-Monotonic (NM) and deep Monotonic Woods-Saxon (MWS) potentials. The Pauli-laden energy density functional (EDF) theory, which results in NM potentials, is also discussed. Equally good fits to the CS, T_{20}, T_{21}, and T_{22} data are obtained using both NM and MWS potentials. But iT_{11} data is only reproduced well using NM potentials in OM. The shallow NM potentials seem better than the deep MWS for simultaneous description of the CS, iT_{11}, T_{20}, T_{21}, and T_{22} data.

Introduction

The best choice of the nuclear interaction potential between two nuclei is a long-standing and challenging problem (Brandan and Satchler, 1997). The study of nucleus-nucleus (NN) potentials is essential not only to understand the structure of the nucleus (Basak et al., 2022) but also for the burning of stars (Duarte et al., 2015) and dynamics of the nucleosynthesis for astrophysics (Thomas, 2020). The exact and reliable NN potential can only lead us to the deep learning of nuclear matter and its structures in the whole universe. The elastic scattering, including diffractive and refractive structures, is significant in obtaining the true nature of NN potentials (Hussain and McVoy, 1948; Hussain and Satchler, 1994; Khoa et al., 2007). The elastic ^{6}Li+^{12}C scattering system also shows diffractive and refractive structures in a wide range of incident energies (Trcka et al., 1990). A few numbers of simultaneous studies are done with the interaction of polarized ^{6}Li on ^{12}C to reproduce the experimental cross section *(CS),* vector analyzing power (VAP) (iT_{11}), and tensor analyzing power (TAP) (T_{20}, T_{21}, and T_{22}) data (Reber et al.,1994; Kerr et al., 1996; Kerr et al., 1995) but none of them have reproduced the data well. Reber et al. (1994) using Woods-Saxon (WS) potentials, showed that the description of the iT_{11} data needs an angular momentum (J)-dependent absorption interaction. Kerr et al. (1995) performed an optical model (OM) analysis of the ^{6}Li+^{12}C elastic scattering at 30 MeV using phenomenological WS potentials, including a J-dependent absorption term. They found that T_{21} arises mainly from the tensor interaction, T_{20} from coupling the J-dependent and tensor interactions, and the most complicated iT_{11} stems from a combination of the spin-orbit, tensor, and J-dependent interactions.

*Corresponding author:<sujan4367@gmail.com>

[1]*Bangladesh Atomic Energy Commission, Dhaka, Bangladesh*

[2]*Department of Physics, University of Rajshahi - Rajshahi, Bangladesh*

There are two types of nuclear potentials used in OM for the real part: the phenomenological optical potential (OP) and the microscopically derived one. The phenomenological OPs directly obtained from the analysis of elastic scattering data are found to suffer from discrete and continuous potential ambiguities (Mohr et al., 1997; Satchler, 1983; Islam et al., 2021a; Islam et al., 2021b; Islam et al., 2021c). It is very challenging to remove ambiguities of potential parameters. The discrete potential ambiguity can only be eliminated in the refractive angular structure at higher energies for all kinds of OPs (Goldberg and Smith, 1972; Goldberg et al., 1973; Khoa et al., 2007; Islam et al., 2021a; Islam et al., 2021b) where the *CS* maximum of the primary nuclear rainbow is followed by an exponential type falloff pattern in the shadow region classically. The microscopic nuclear potentials such as Double Folding (DF) (Satchler and Love, 1979) and Non-Monotonic (NM) (Basak et al., 2011) are directly derived from the microscopic theories. The DF potentials for the Li-nucleus elastic scattering need a significant renormalization factor of $N_R 0.5 - 0.6$ (Pakou, 2008) in the simple OM to reproduce the *CS* data and lead to a complete failure to explain the opposite signs of vector analyzing power (iT_{11}) for the ^{6,7}Li elastic scattering. However, all nuclear potentials can be grouped into Monotonic and Non-Monotonic (NM), respectively, without and with repulsive potential at the core. The schematic difference between Monotonic and NM potentials is shown in Fig. 1. The NM potentials are derived from the EDF theory of Brueckner et al. (1968) which incorporates appropriately the Pauli-principle and the derived potentials become shallow in terms of volume integral per nucleon pair ($J_R/A_P A_T$), A_P and A_T being the mass numbers of the projectile and target nuclei, respectively. Familiar Woods-Saxon (WS) (Woods and Saxon, 1954), Squared Woods-Saxon (SWS) (Michel et al., 1983), and widely used double folding (DF) (Satchler and Love, 1979) potentials are monotonic and deep.

The microscopic NM potential with a repulsive core derived from the EDF theory of (Brueckner et al., 1968a; Brueckner et al., 1969) (BCD) which incorporates appropriately the Pauli principle enjoyed several successes in recent years which include: (*i*) the alpha-elastic scattering (Tariq et al., 1999), (*ii*) alpha-inelastic scattering (Basak et al., 2001), (*iii*) one- (Das et al., 1999), two- (Das et. al., 2000a; Das et al., 2001), three-nucleon (Das et al., 2000b) transfer reactions, (*iv*) band-mixing of band heads $I^\pi = 1/2^+$ and $I^\pi = 3/2^+$in the Nilsson model (Hossain et al., 2005), (*v*) verification of the Goldberg criterion (Goldberg and Smith, 1972) of the ^{16}O+^{16}O (Islam et al., 2021a) and ^{12}C+^{12}C (Islam et al., 2021b) elastic scattering with discussion on the intriguing aspect at potential families at lower energies, (vi) ^{16}O+^{16}O cluster states and their fusion to ^{32}S (Basak et al., 2022), (vii) a novel method (Hossain et al., 2015) for determining the nuclear incompressibility *K* for cold nuclear matter using the ^{16}O+^{16}O elastic scattering. (viii) The opposite signs of the vector analyzing power (VAP) of ^{6,7}Li elastic scattering by ^{58}Ni at 20 MeV (Basak et al., 2011) and ^{120}Sn at 44 MeV (Basak et al., 2011) are reproduced successfully using NM potentials in the OM. This result eliminates a long-standing puzzle. (ix) The NM potential also reveals explicitly the multiple potential families (Islam et al., 2021a; Islam et al., 2021b) at low energies, which can produce an excellent description of elastic experimental data over an extensive angular range.

In the present investigation, the elastic ^{6}Li+^{12}C experimental differential CS, iT_{11}, T_{20}, T_{21}, and T_{22} data at the incident laboratory energy of 30 MeV are analyzed within the structure of the OM using shallow NM and deep Monotonic Woods-Saxon (MWS) (Woods and Saxon, 1954) OPs without including *J*-dependent absorption term. The present article also discusses the Pauli-laden BCD's EDF (Brueckner et al., 1968a) for deriving the NM potentials. The results obtained using both the NM and MWS potentials are compared. The latter uses the Woods-Saxon form factor (Woods and Saxon, 1954).

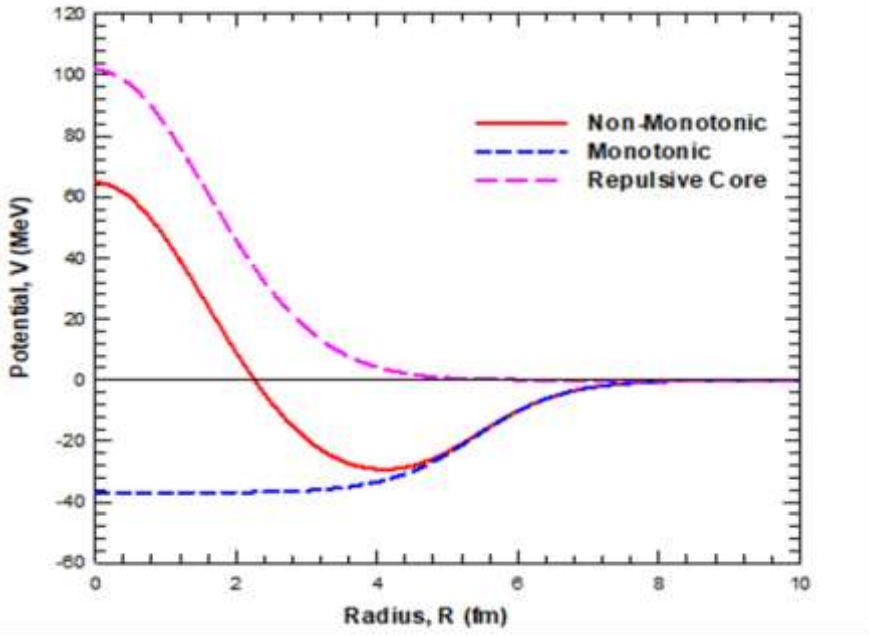

Fig. 1. A schematic difference between Monotonic (dashed blue line) and Non-Monotonic (solid red line) potentials, respectively, without and with repulsive core (pink medium dashed line).

Optical Model Potentials

Energy Density Functional (EDF) Theory

The energy of a nucleus in the EDF theory (Brueckner et al., 1968a) is expressed in terms of density distribution $\rho(r)$ as

$$E = \int \varepsilon[\rho(\boldsymbol{r})]\mathrm{d}^3\boldsymbol{r} \tag{1}$$

where, the energy density $\boldsymbol{\epsilon[\rho(r)]}$ is given by

$$\boldsymbol{\epsilon[\rho(r)] = 0.3\left(\frac{\hbar}{2M}\right)\left(\frac{3\pi^2}{2}\right)^{\frac{2}{3}}[1-\xi)^{\frac{5}{3}} + (1+\xi)^{\frac{5}{3}}] \times \rho^{\frac{5}{3}} + \nu(\rho,\xi)\rho + \frac{e}{2}\emptyset_C(r)\rho_p - 0.739e^2\rho_p^{\frac{4}{3}} + \left(\frac{\hbar^2}{8M}\right)} \tag{2}$$

Here, M represents the mass of a nucleon, and $\xi = (N-Z)/A$ represents the neutron excess parameter. The first term in (2) arises from the nucleon kinetic energy in nuclear matter. The second term is determined from the Gammel-Christian-Thaler (GCT) nucleon-nucleon (n-n) potential (Brueckner and Gammel,1958) in the Brueckner-Hartree-Fock (BHF) theory. The GCT potential is formed by the combination of central, spin-orbit, and tensor potential parts of the realistic n-n potential, which can describe all the properties of deuteron and the n-n scattering data up to the pion threshold (~137 MeV). In the BHF theory, the mean-field relates the matrix elements of the n-n potential (Brueckner et al., 1968a) to those of the scattering operator with full consideration of the Pauli principle among the nucleons of the same type in the nuclear and nucleonic matter approximations, i.e., using the plane wave for nucleonic wave functions. The third term represents the Coulomb energy, and the fourth term is the correction of Coulomb energy due to the consideration of the Pauli principle among protons (Brueckner et al., 1968b; Hossain et al., 2015). The last term arises due to the inhomogeneity correction (Brueckner et al.,1968b; Hossain et al., 2015) to the kinetic energy due to the finite size and correlation effect among nucleons. The density dependence of the energy per nucleon, *E/A*, in the nuclear and nucleonic matter using the BGT n-n potential with full consideration of the Pauli principle has been calculated in (Brueckner et al. 1968a, Hossain et al., 2015).

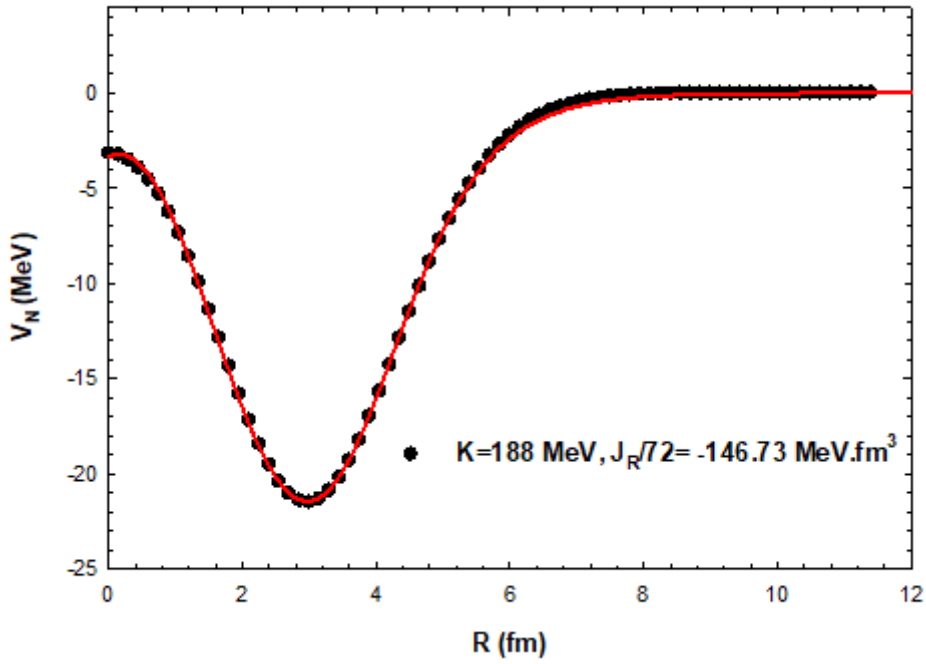

Fig. 2. Parameterization of EDF-generated nuclear potential points for *K*=188. The parameters are listed in Table 1.

Table 1. The equivalent 2pF DDFs parameters for ^{6}Li and ^{12}C.

Nucleus	2pF DD Function parameters			Binding Energy	
	c (fm)	*z* (fm)	ρ_0 (fm^{-3})	Calculated (MeV)	Experimental (MeV)
^{6}Li	1.333	0.577	0.2118	33.2	32.0
^{12}C	2.294	0.434	0.1752	92.0	92.2

The density dependence of the mean-field $v(\rho,\xi)$ for a symmetric (ξ=0) and homogeneous part of a finite nucleus has been parameterized analytically (Hossain et al., 2015) as

$$v(\rho,\xi=0)=\lambda_1\rho+\lambda_2\rho^{4/3}+\lambda_3\rho^{5/3} \quad (3)$$

Here, the values of the mean-field parameters for *K*= 188 MeV are

$\lambda_1=-741.28, \lambda_2=+1179.55,$ and $\lambda_3=-467.54,$ as given in (Hossain et al., 2015).

The EDF potential *V(R)* between the projectile and the target at an interaction distance of *R* is given by

$$V(R)=E[\rho(\boldsymbol{r},R)]-E[\rho_P(\boldsymbol{r},R=\infty)]-E[\rho_T(\boldsymbol{r},R=\infty)] \quad (4)$$

Here, ρ represents the composite nucleus's density distribution function (DDF). And ρ_P and ρ_T represents the DDFs for the projectile and the target at *R*= ∞, respectively. The DDF of the composite nucleus in the sudden approximation is given as

$$\rho(\boldsymbol{r})=\rho_P(\boldsymbol{r})+\rho_T(\boldsymbol{r}) \quad (5)$$

The sources of density distribution functions (DDFs) are for ^{6}Li from (Bray et al., 1972) and ^{12}C from (Sick, 1974). These DDFs are re-parametrized by the two-parameter Fermi (2pF) function for application to the EDF calculation as

$$\rho(\boldsymbol{r})=\rho_0[1+\exp\left(\frac{r-c}{z}\right)]^{-1} \quad (6)$$

Table 1 shows the obtained parameters from the equivalent 2pF DDFs for ^{6}Li and ^{12}C and the calculated and experimental binding energies. The calculated EDF potentials are depicted as points in Fig. 2.

Non-monotonic (NM) Potentials Forms

The EDF-derived NM nuclear part of the ^{6}Li-^{12}C potential points has been parameterized with the following functional forms:

$$V_{NM}(R) = -V_0\left[1+exp\left(\frac{R-R_0}{a_0}\right)\right]^{-1} + V_1\, exp\left[-\left(\frac{R-D_1}{R_1}\right)^2\right] \quad (7)$$

The imaginary part of the ^{6}Li+^{12}C OP is taken phenomenologically (Hossain et al., 2015) as

$$W_{NM}(R) = -W_0 exp\left[-\left(\frac{R}{R_W}\right)\right]^2 - W_S\, exp\left[-\left(\frac{R-D_S}{R_S}\right)^2\right] \quad (8)$$

Monotonic Woods-Saxon (MWS) Potentials

The fundamental part of the ^{6}Li+^{12}C MWS (Woods and Saxon, 1954) potential is taken phenomenologically to be composed of only attractive parts as

$$V_{MWS}(R) = -V_0\left[1+exp\left(\frac{R-R_0}{a_0}\right)\right]^{-1} \quad (9)$$

The phenomenological imaginary part of the MWS potential is assumed to be composed of a WS-shaped (Woods and Saxon, 1954) volume term and a surface term in the shifted Gaussian form (Hossain et al., 2015) as:

$$W_{MWS}(R) = -W_0[1+\exp(\frac{R-R_W}{a_w})]^{-1} - W_S exp\left[-\left(\frac{R-D_S}{R_S}\right)^2\right] \quad (10)$$

Spin-orbit, Tensor, and Coulomb Potentials used in OM potentials

An effective spin-orbit, U_{SO}(R) part, and a tensor part, U_T(R) in OPs following Reber et al., (1994) and Kerr et al., (1995) are taken in the standard WS as:

$$U_{so}(R) = 2.0\frac{V_{so}}{R}\frac{d}{dR}[1+\exp\left(\frac{\mathrm{R-R_{so}}}{\mathrm{a_{so}}}\right)]^{-1}\, l.I \quad (11)$$

$$U_T(R) = 8\left[V_T a_{RT}^2 \frac{d^2}{dR^2}[1+\exp\left(\frac{R-R_{RT}}{a_{RT}}\right)]^{-1}\right]\times \left[\left(\boldsymbol{I}.\check{\mathrm{R}}\right)^2-\frac{2}{3}\right] \quad (12)$$

In equations (11 and 12), ℓ, $\boldsymbol{I}$, and $\check{\mathrm{R}}$ refer, respectively, to the partial wave angular momentum, ^{6}Li-spin operators, and a unit vector along increasing R. The factor 2.0 in equation (11) stems from $(\hbar/m_\pi c)^2 = 2.0$ fm^2, and a factor $6\sqrt{3}$ in equation (12) has been omitted to conform to the algorithm in the code FRESCO (Thompson, 1988).

The Coulomb potential V_C(R) is taken as,

$$V_C(R) = \begin{cases} \frac{1}{4\pi\epsilon_0}\frac{Z_P Z_T e^2}{R}, & R \geq R_C \\ \frac{1}{4\pi\epsilon_0}\frac{Z_P Z_T e^2}{2R_C}\left(3-\frac{R^2}{R_C^2}\right), & R < R_C \end{cases} \quad (13)$$

Here, R_C is the Coulomb radius of a uniformly charged sphere.

The resultant forms of the NM and MSW OPs stand, respectively, as

$$U^{NM}(R) = V_C(R) + V_{NM}(R) + W_{NM}(R) + U_{so}(R) + U_T(R) \quad (14)$$

and

$$U^{MWS}(R) = V_C(R) + V_{MWS}(R) + W_{MWS}(R) + U_{so}(R) + U_T(R) \quad (15)$$

Analysis and Results

The data of experimental CS and analyzing powers (iT_{11}, T_{20}, T_{21}, and T_{22}) for the ^{6}Li+^{12}C elastic scattering at 30 MeV are taken from (Kerr et al., 1995). A systematic error of 15% is considered for the experimental data points. The Coulomb radius R_C = 3.92 fm is taken to calculate the Coulomb potential in equation (13). All calculations of OM are performed using the code SFRESCO, which includes the coupled-channels code FRESCO2.9 (Thompson,

1988) and the χ^2-minimization code MINUIT (James and Roos, 1975). The fitting parameters are determined by minimizing the χ^2 expressed by.

$$\chi^2 = \frac{1}{N-F}\sum_i \left[\frac{\sigma_{exp}(\theta_i)-\sigma_{th}(\theta_i)}{\Delta\sigma_{exp}(\theta_i)}\right]^2 \quad (16)$$

Here $\sigma(\theta)$ and $\Delta\sigma(\theta)$ represent the cross-section and the corresponding error at the scattering angle θ. F represents the number of experimental data points, and N is the number of adjusted parameters. N-F denotes the degrees of freedom in minimizing the χ^2 for the data fitting.

In the initial step of the OM analysis, the EDF-derived NM potential parameters for the real part listed in Table 2 were fixed. The parameters of the imaginary parameters of W_{NM} in equation (8) were searched to obtain the best fit to the CS data only with χ^2=388. The EDF potential is valid at the zero-excitation energy $E_x = 0$ (Islam et al., 2021a; Islam et al., 2021b) of the composite nucleus ^{18}Ar. No energy dependency parameter is found from the derivation of NM potential from EDF theory. Hence, the EDF-generated NM potential parameters needed to be readjusted for a good description of the CS data at 30 MeV. Therefore, successive grid and global searches on both the EDF–generated V_{NM} parameters in Table 2 and the previously optimized $W_{\rm NM}$ parameter were employed to describe the *CS* data accurately.

In the next step, the spin-orbit potential parameters (V_{SO}, R_{SO}, and a_{SO}) in equation (11) and the central imaginary parameters optimized in the previous step were adjusted empirically on the iT_{11} data employing a successive number of grid searches. In the third step, the tensor potential parameters (V_T, R_T, and a_T) were employed in a successive number of grid searches to reproduce the T_{21} data.

In the final step, all parameters of equation (14), except the constancy of R_C=3.92 fm, were tuned in values with a successive number of grid searches to reproduce well the experimental CS and analyzing powers (iT_{11}, T_{20}, T_{21}, and T_{22}) data simultaneously. The final fits are done by visually inspecting the angular structure of the experimental data because it is essential to reproduce the angular distributions when $\chi^2 \gg 1$. (Perey, 1963; Koning and Delaroche, 2003). All the parameters obtained from the best fitting are shown in Tables 2 and 3. The χ^2 and the volume integrals J_R/72 and J_I/72, respectively, for the real and imaginary parts of the OP, are also listed in Tables 2 and 3. The calculated *CS* and analyzing powers (iT_{11}, T_{20}, T_{21}, and T_{22}) shown in the red solid lines using the NM potentials compare well with the experimental data in Fig. 3.

Table 2. Parameters of the nuclear real and spin-orbit parts of OP at 30 MeV.

Type	V_0 (MeV)	R_0 (fm)	a_0 (fm)	V_1 (MeV)	R_1 (fm)	D_1 (fm)	V_{SO} (MeV)	R_{SO} (fm)	a_{SO} (fm)	$J_R/72$ (MeV.fm3)	χ^2
EDF	39.19	3.94	0.766	-35.72	2.43	0.133	-	-	-	-146.73	-
NM	57.12	3.94	0.710	-198.4	1.92	0.133	0.50	5.26	0.55	-144.83	45.0
MWS	300.0	2.22	0.840	-	-	-	1.30	2.75	0.65	-465.16	146.2

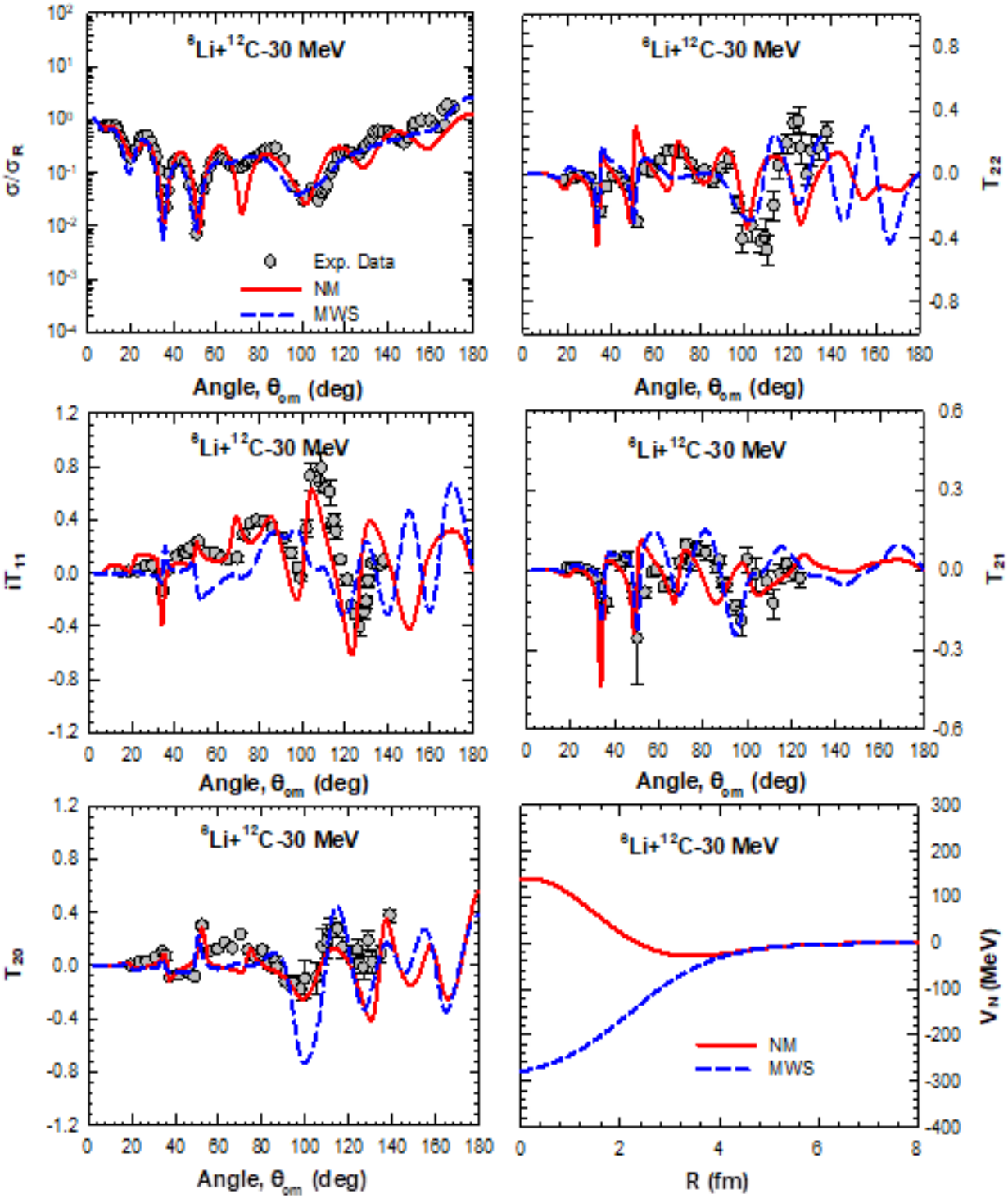

Fig. 3. Optical model (OM) calculations using NM potential (red solid lines) and MWS potential (blue dashed lines) are compared to the experimental *CS* and analyzing powers (iT_{11}, T_{20}, T_{21}, and T_{22}) data of ^{6}Li+^{12}C at 30 MeV using the OP parameters, listed in Table 2 and 3. The radial distributions of nuclear real parts of the two types of OP potential are also displayed in the last inset.

Table 3. Same as Table 2 but for the imaginary and tensor interaction parts.

Type	W_0 (MeV)	R_W (fm)	a_W (fm)	W_S (MeV)	D_S (fm)	R_S (fm)	V_T (fm)	R_T (fm)	a_T (fm)	$J_I/72$ (MeV.fm3)
NM	17.2	3.80	-	15.5	4.40	0.12	2.0	3.94	0.72	-83.92
MWS	17.3	3.11	1.18	0.50	4.92	0.60	2.0	4.58	0.30	-76.25

The above-mentioned fitting procedure was repeated for the U^{MWS} potential in equation (15), with its fundamental part V_{MWS} lacking in the repulsive core (see equation (9)). The initial parameters of the real nuclear part of U^{MWS} were taken from (Kerr et al., 1995). The best-fit parameters using U^{MWS} potentials are also displayed in Tables 2 and 3. The value of χ^2 and the volume integrals $J_R/72$ and $J_I/72$ of equation (15), respectively, for the real and imaginary OP parts, are also listed in Tables 2 and 3. The predicted results of the *CS* and analyzing powers (iT_{11}, T_{20}, T_{21}, and T_{22}) using the U^{MWS} potentials at 30 MeV, shown in the blue dashed lines, are compared to the experimental data in the same Fig. 3. The comparison of nuclear real parts of both the NM and MWS potentials is also shown graphically in Fig. 3.

It is observed from Fig. 3 that the experimental data on the elastic ^{6}Li+^{12}C scattering *CS* along with T_{20}, T_{21}, and T_{22} are reproduced overall successfully at energy 30 MeV in the framework of the simple optical model using both the shallow NM and deep MWS potentials without the J-dependent absorption. However, the iT_{11} data is only well reproduced using shallow NM potential. The MWS potential cannot produce the exact angular shape and position of iT_{11} data well at the mid and higher angular regions. The $J_R/72$ value of NM potential is found to be -144.83 MeV.fm^3, slightly lower than the value of -146.73 MeV.fm^3 for the EDF-derived potential. On the other hand, the value of $J_R/72$ =- 465.16 MeV.fm^3 for MWS is found to be very deep compared to the value of the actual volume integral found in NM potential. For the overall fitting value for *CS*, iT_{11}, T_{20}, T_{21}, and T_{22}, the average chi-square is found using NM potentials to be only χ^2 = 45.0, but for MWS potentials, the χ^2 = 146.2, which is much larger than the NM description. The higher value of $J_R/72$ for MWS compared to the NM potentials suggests the MWS potential is very deep. However, based on two observations: (*i*) the visual inspection of the theoretical description of experimental angular structures of *CS*, iT_{11}, T_{20}, T_{21}, and T_{22} in Fig. 3 and (*ii*) a comparison of the χ^2 values found for both NM and MWS potentials in Table 2, we can suggest the following. The simultaneous analysis using a simple OM picture is found to be much better for the shallow NM potential than the deep MWS potential.

Discussions and Conclusions

The investigation reports the comparative and simultaneous description of the experimental *CS*, iT_{11}, T_{20}, T_{21}, and T_{22} data of the ^{6}Li elastic scattering by ^{12}C at 30 MeV in the structure of simple OM picture using shallow NM and deep MWS potentials. The MWS potential can simultaneously describe the *CS*, T_{20}, T_{21}, and T_{22} data except iT_{11} data in a simple OM picture. On the other hand, the shallow NM potential can successfully describe and also simultaneously all the data sets (*CS*, T_{20}, iT_{11}, T_{21}, and T_{22}) in OM, as shown in Fig. 3. The overall image of the simultaneous description of CS and all the analyzing powers (APs) using the shallow NM potential seems much better than the description using the MWS one.

Our simple optical model description of the *CS* and APs using NM potentials without a *J*-dependent absorption plays better than the description using the *J*-dependent absorption reported in (Reber et al., 1994; Kerr et al., 1995) and also the findings from the Coupled-Channels (CC) calculations in (Reber et al., 1994; Kerr et al., 1995; Kerr et al., 1996). The present analysis using the simple OM suggests that the *J*-dependent absorption potential is *non-essential* for describing the VAP and TAP data. The present investigation with the NM potential shows that the best choice for simultaneous examination of the vector and tensor effects in NN interactions is the repulsive core arising from the Pauli effect. Moreover, the key to success in the simultaneous analysis of CS and analyzing powers using the shallow NM potential rather than deep MWS potential lies in the appropriate generation of a dynamic polarization potential (DPP) effect (Brandan and Satchler, 1997), even in the framework of OM. The appropriate DPP effect with the NM potentials from BCD's EDF (Brueckner et al., 1968a) stems from the realistic n-n potential of GCT (Brueckner and Gammel, 1958), which involves the spin- and tensor-interactions apart from the central part.

Another essential feature of the EDF-derived NM potentials at low energies is their energy independence (Islam et al., 2021a; Islam et al., 2021b). This aspect of the EDF potentials bears excellent promise in employing the NM potentials for studying the NN fusion at the astrophysical low-energies where reliable potentials are scarce. We are now examining the NM potentials on the $^{16}O+^{16}O$, $^{16}O+^{12}C$, and $^{12}C+^{12}C$ fusion reactions at deep sub-Coulomb energies, which play an essential role in stellar evolution and supernovae explosions.

Acknowledgment

The authors wish to thank Dr. Ian J. Thompson for his code FRESCO.

References

Basak AK, Abdullah MNA, Tariq ASB, Das SK, Rahman AFMN, Mondal AS, Sen Gupta HM and Malik FB. Investigation of inelastic α-scattering on ^{24}Mg and ^{28}Si. *The Eur. Phys. J. A.* 2001; 12(4): 387-397.

Basak AK, Billah MM, Kobra MJ, Sarkar MK, Rahman MM, Das PK, S. Hossain S, Abdullah MNA, Tariq ASB and Uddin MA. Non-monotonic potentials and vector analyzing powers of ^{6,7}Li scattering by ^{12}C, ^{26}Mg, ^{58}Ni, and ^{120}Sn. *Europhys. Lett*. 2011; 94(6): 62002.

Basak AK, Merchant AC, Freer M, Islam MS, Ramon RA, Rahman MM, Tariq ASB, Uddin MA and Soylu A. $^{16}O + ^{16}O$ cluster states and their fusion to ^{32}S: A non-monotonic potential description. *Europhys. Lett*. 2022; 138(4)**:** 44002.

Brandan ME and Satchler GR. The interaction between light heavy-ions and what it tells us. *Phys. Rep.* 1997; 285 (4-5): 143-243.

Bray KH, Mahavir jain, Jayaraman KS, Lobianco G, Moss GA, Van Oers WTH, Wells DO and Petrovich F. Elastic and inelastic scattering of protons from ^{6}Li between 25 and 45 MeV. *Nucl. Phys. A*. 1972; 189(1): 35-64.

Brueckner KA and Gammel JL. Properties of nuclear matter, *Phys. Rev*. 1958; 109(4): 1023-1039.

Brueckner KA, Buchler JR, Clark RC and Lombard RJ. Statistical theory of nuclei. II. Medium and heavy nuclei. *Phys. Rev.*1969; 181(4): 1543-1551.

Brueckner KA, Buchler JR, Jorna S and Lombard RJ. Statistical theory of nuclei, *Phys. Rev*. 1968b; 171(4): 1188-1195.

Brueckner KA, Coon SA, and Dabrowski J. Nuclear symmetry energy. *Phys. Rev*. 1968a; 168(4): 1184-1188.

Das SK, Basak AK, Banu K, Mondal AS, Tariq ASB, Rahman AFMN, Gupta HMS, and Malik FB. Effect of the α-nucleus potential on the ^{28}Si

(α, p)^{31}P reaction. *Phys. Rev. C.* 2000b; 62(5): 054606.

Das SK, Tariq ASB, Rahman AFMM, Roy PK, Huda MN, Mondal AS, Basak AK, Gupta HMS and Malik FB. Effect of α-nucleus potential on the ^{27}Al (α, t) ^{28}Si reaction, *Phys. Rev. C.* 1999; 60(4): 044617.

Das SK, Tariq ASB, Rahman AFMN, Hossain S, Mondal AS, Basak AK, Gupta HMS and Malik FB. Effect of the α-nucleus interaction on the ^{29,30}Si (α, d)^{31,32}P reaction. *Phys. Rev. C.* 2001; 64(3): 034605.

Das SK, Tariq ASB, Uddin MA, Mondal AS, Basak AK, Rashid KM, Gupta HMS and Malik FB. Effect of α-nucleus potential on the ^{28}Si (α, d) ^{30}P reaction. *Phys. Rev. C.* 2000a; 62 (5): 054605.

Duarte JG, Gasques LR, Oliveira RB, Zagatto VAB, Chamon LC, Medina NH, Added N, Seale WA, Alcántara-Núñez JA, Rossi Jr ES, Amador-Valenzuela P, Lépine-Szily A, Freitas AS, Scarduelli V, Aguiar VAP[1] and Shorto JMB. Measurement of fusion cross sections for ^{16}O+^{16}O, *Phys. G: Nucl. Part. Phys.* 2015; 42(6): 065102.

Goldberg DA and Smith SM. Criteria for the elimination of discrete ambiguities in nuclear optical potentials. *Phys. Rev. Lett.* 1972; 29(8): 500-503.

Goldberg DA, Smith SM, Pugh HG, Roos PG and Wall NS. Scattering of 139-MeV Alpha Particles by ^{58}Ni and ^{208}Pb. *Phys. Rev. C.* 1973; 7(5): 1938-1950.

Hossain S, Abdullah MNA, Das SK, Uddin MA, Basak AK, Gupta HMS, Thompson IJ and Malik FB. Band mixing in ^{29}Si and ^{29}P. *J. Phys. G: Nucl. Part. Phys.* 2005; 31(5): 309.

Hossain S, Tariq ASB, Nilima A, Islam MS, Majumder R, Sayed MA, Billah MM, Azad MMB, Uddin MA, Reichstein I, Malik FB and Basak AK. Dependence of the ^{16}O+^{16}O nuclear potential on nuclear incompressibility. *Phys. Rev. C.* 2015; 91(6): 064613.

Islam MS, Majumder R, Hossain S, Nilima A, Sayed MA, Islam MS, Billah MM, Azad MMB, Tariq ASB and Uddin MA. Non-monotonic shallow nucleus-nucleus potential for heavy-ion elastic scattering. *J. Phys.: Conf. Ser.* 2021c; 1718: 012009.

Islam MS, Ramon RA, Rahman MM, Islam MS, Azad MMB, Tariq ASB, Uddin MA, Ali S and Basak AK. Primary rainbow and Airy minima in ^{12}C +^{12}C elastic scattering with families of non-monotonic potentials. *J. Phys. G: Nucl. Part. Phys.* 2021b; 48(12): 125108.

Islam MS, Ramon RA, Rahman MM, Majumder R, Sayed MA, Nilima A, Azad MMB, Tariq ASB, Uddin MA and Basak AK. Nature of potential families from elastic ^{16}O +^{16}O rainbow scattering. *J. Phys. G: Nucl. Part. Phys.* 2021a; 48(7): 075109.

James F and Roos M. Minuit - a system for function minimization and analysis of the parameter errors and correlations. *Comput. Phys. Comm.*1975; 10: 343-367.

Kerr PL, Kemper KW, Green PV, Mohajeri K, Myers EG, Robson D and Schmidt BG. Tensor effects in ^{6}Li→+^{12}C scattering. *Phys. Rev. C.* 1995; 52(4):1924-1933.

Kerr PL, Kemper KW, Green PV, Mohajeri K, Myers EG, Schmidt BG and Hnizdo V. ^{6}Li→+^{12}C inelastic scattering at 30 and 50 MeV. *Phys. Rev. C* 1996; 54(3): 1267-1281.

Khoa DT, Oertzen Wv, Bohlen HG and Ohkubo S. Nuclear rainbow scattering and nucleus–nucleus potential. *J. Phys. G: Nucl. Part. Phys.* 2007; 34(3): R111-R164.

Koning AP and Delaroche JP. Local and global nucleon optical models from 1 keV to 200 MeV. *Nucl. Phys. A.* 2003; 713(3-4): 231-310.

Michel F, Albinski J, Belery P, Delbar TH, Grégoire Gh, Tasiaux B and Reidemeister G. Optical model description of α+^{16}O elastic scattering and

alpha-cluster structure in ^{20}Ne. *Phys. Rev. C.* 1983; 28: 1904-1917.

Mohr P, Rauscher T, Oberhummer H, Máté Z, Fülöp Zs, Somorjai E, Jaeger M and Staudt G. ^{144}Sm-α optical potential at astrophysically relevant energies derived from ^{144}Sm(α,α)^{144}Sm elastic scattering. *Phys. Rev. C.* 1997; 55(3):1523-1531.

Pakou A. Polarization potential for elastic scattering of ^{6,7}Li + ^{28}Si at near-barrier energies. *Phys. Rev. C*. 2008; 78(6): 067601.

Perey FG. Optical-model analysis of proton elastic scattering in the range of 9 to 22 MeV. *Phys. Rev*. 1963, 131(2):745-763.

Reber EL, Kemper KW, Green PV, Kerr PL, Mendez AJ, Myers EG and Schmidt BG. Spin-orbit and tensor potentials from polarized ^{6}Li scattering. *Phys. Rev. C. Nucl. Phys.* 1994; 49(1): R1-R4.

Reber EL, Kemper KW, Green PV, Kerr PL, Mendez AJ, Myers EG, Schmidt BG and Hnizdo V. Analysing powers for elastic and inelastic scattering of polarized ^{6}Li from ^{12}C at 30 MeV. *Phys. Rev. C. Nucl. Phys.*1994; 50(6):2917-2926.

Satchler GR. Direct nuclear reactions. Clarendon Press: Oxford, UK. 1983. p. 854.

Satchler GR and Love WG. Folding model potentials from realistic interactions for heavy-ion scattering. *Phys. Rep.* 1979; 55(3): 183-254.

Sick I. Model-independent nuclear charge densities from elastic electron scattering. *Nucl. Phys. A.* 1974; 218: 509-541.

Tariq ASB, Rahman AFMM, Das SK, Mondal AS, Uddin MA, Basak AK, Gupta HMS and Malik FB. Potential description of anomalous large angle scattering of α particles. *Phys. Rev. C.* 1999; 59(5): 2558-2566.

Thomas R. Essentials of nucleosynthesis and theoretical nuclear astrophysics. IOP Publishing Ltd. 2020. p. 450.

Thompson IJ. Coupled reaction channels calculations in nuclear physics. *Comput. Phys. Rep*. 1988; 7(4): 167-212.

Trcka DE, Frawley AD, Kemper KW, Robson D, Fox JD and Myers EG. Angular momentum dependent absorption in ^{6}Li scattering. *Phys. Rev. C* 1990; 41: 2134-2146.

Woods RD and Saxon DS. Diffuse surface optical model for nucleon-nuclei scattering. *Phys. Rev*. 1954; 95: 577-578.